

Anti-corrosive Properties of CeO₂ Conversion Coatings on Aluminum Alloy 2024 Prepared by Dip Immersion Method

Niloufar Bahramipناه¹, Iman Danaee^{2*}, Maryam Kanani³, and Mohammad Hosein Maddahy⁴

¹ Assistant Professor, Department of Chemistry, Payame Noor University, P.O.BOX 19395-3697, Tehran, Iran

² Associate Professor, Department of Petroleum Engineering, Petroleum University of Technology, Abadan, Iran

³ M.S. Student, Department of Petroleum Engineering, Petroleum University of Technology, Abadan, Iran

⁴ M.S. Student, Department of Petroleum Engineering, Petroleum University of Technology, Abadan, Iran

Received: July 30, 2014; *revised:* December 16, 2014; *accepted:* February 09, 2015

Abstract

As an alternative to chromate conversion coatings, rare-earth coatings especially cerium, because of the low toxicity, have attracted considerable attention. Using dip immersion method, cerium-based conversion coating was deposited on aluminum 2024. Corrosion resistance was studied in 3.5 wt.% NaCl solution using potentiodynamic polarization, electrochemical impedance spectroscopy, and surface methods. The coated samples revealed a considerable decrease in corrosion rate and with increasing immersion time up to 1200 s, the coating resistance increased. Electrochemical impedance data showed that the aluminum charge transfer resistance was increased in the existence of cerium oxide conversion coatings. Using energy dispersive spectroscopy (EDS) and scanning electron microscopy (SEM), the chemical composition and surface morphology were also evaluated.

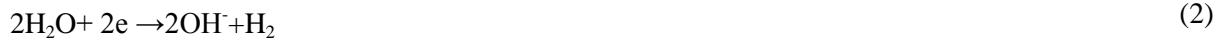
Keywords: Aluminum 2024, Cerium Oxide Conversion Coatings, Impedance, Corrosion, SEM

1. Introduction

As a structural material, aluminum is extensively applied due to its good properties such as corrosion resistance, good strength-to-weight ratio, and low cost. Also, because of its low density, aluminum is used in aerospace, military, and industry. Aluminum needs alloying in order to develop high strength and to decline the aluminum corrosion characteristics. Due to the second phase particles in alloys, a potential difference between alloy element and aluminum matrix is generated. Therefore, followed by a decline in the corrosion resistance of aluminum, especially against halide ions, a galvanic cell is formed (Brunelli et al., 2009). Conventionally, chromate conversion coatings have been largely used to prevent aluminum alloys from corrosion (Johansen et al., 2012). However, the compounds of hexavalent chromium are greatly carcinogenic and toxic. Amongst the alternatives, rare-earth coatings, especially cerium, have attracted considerable attention (Conde et al., 2008). Stable hydroxide and oxide film is formed by cerium, which is non-toxic and inexpensive. The mechanism

* Corresponding Author:
Email: danaee@put.ac.ir

of deposition includes both the oxidation of aluminum and H₂O₂ reduction as follows (Rivera et al., 2004):



H₂O₂ is added as an effective accelerator additive. The acceleration provided by the H₂O₂ may be because of the fast increase in pH caused by a reduction in H₂O₂, which would improve the cerium oxide and cerium hydroxide deposition (Johnson et al., 2005). Considering the Pourbaix diagram, at a lower pH, Ce(III) is more stable; therefore, Ce(IV) is reduced to Ce(III). However, in a higher pH range, Ce(IV) would be more stable, especially when oxidizing agents such as O₂ or H₂O₂ are available (Campestrini et al., 2002). On aluminum 2024T3, a previous study has explained the effect of different deposition methods like brush, sol gel, and spray coatings on the corrosion resistance of cerium based conversion coatings (Pinc et al., 2009; Pinc et al., 2010; Tang et al., 2011; de Frutos et al., 2008). Tang et al. has shown that the application of brush plated conversion coatings based on cerium oxide on AA2024-T3 alloys improves corrosion resistance. Moreover, the influence of plating parameters on the corrosion resistance of cerium oxide based coatings was studied.

This study deals with the corrosion properties of 2024-T3 aluminum alloy coated with cerium using dip immersion process through potentiodynamic polarization and impedance spectroscopy. Using scanning electron microscopy and energy dispersive spectroscopy, the surface morphology and chemical composition of the cerium-based conversion coating were evaluated.

2. Experimental

2.1. Substrate preparation

Cerium-based conversion coating were deposited on AA2024 aluminum alloy with the chemical composition of Si: 0.4, Fe: 0.4, Cu: 4, Mn: 0.5, Mg: 1.6, Cr: 0.1, Zn: 0.25, Ti: 0.15, V: 0.05, Zr: 0.05, others: 0.15 wt.%; Al is the balance. From larger panels, the specimens were cut to 1 cm × 1 cm samples. Prior to surface pretreatments, the samples were mounted using epoxy resin. Employing abrasive papers, aluminum coupons were mechanically abraded (400-2000 mesh). The specimens were rinsed with acetone, de-smutted, and alkaline cleaned by soaking in a 1 M NaOH solution for 30 s; then, the panels were acid activated in a 1 M H₂SO₄ solution for 30 s. Between each pretreatment process step, the samples were rinsed with deionized water.

Using dip immersion process, cerium conversion coatings were obtained. The pretreated samples were immersed at room temperature in a cerium solution for times in the range of 30 to 1800 s. The coating bath included 3 drops glycerin, 1 gr. CeCl₃, and 2 ml H₂O₂ in 100 mL de-ionized water. After coating preparation, they were stored at room temperature for 24 hours.

2.2. Methods

The corrosion behavior of the cerium-based conversion coatings was evaluated by using polarization curves and electrochemical impedance spectroscopy (EIS). The solution pH adjustment was performed by the addition of sodium hydroxide or hydrochloric acid. For the electrochemical tests, a three-electrode cell system (PGSTAT 302N) was applied. Ag/AgCl, AA2024, and platinum working electrode were applied as the reference, the working electrode, and the counter respectively. At a rate of 1 mV s^{-1} , the potential was scanned. The following equation was used to calculate polarization resistance:

$$R_p = \frac{\beta_a \beta_c}{2.303(\beta_a + \beta_c)} \cdot \frac{1}{I_{corr}} \quad (6)$$

where, (R_p) is polarization resistance; (I_{corr}) represents corrosion current density, and (β_a , β_c) are Tafel slopes.

For EIS measurements, a frequency sweep from 100 kHz to 10 mHz was utilized. The experimental impedance spectroscopy data fitting to the suggested equivalent circuit was performed using a home written least square software according to the Marquardt method for the functions and Macdonald weighting optimization for the imaginary and real components of the impedance (Macdonald, 1984). Scanning electron microscopy (SEM, VEGA, TESCAN-LMU) equipped with energy dispersive spectroscopy (EDS) was used for characterizing the average chemical composition and surface morphology.

3. Results and discussion

3.1. Surface analysis

The morphologies of the untreated AA2024 aluminum alloy are shown in Figure 1a. The untreated alloy surface was smooth because of the mechanical polishing and chemical etching by NaOH and H_2SO_4 solution. Figure 1b presents the aluminum cerium conversion coatings achieved in an immersion time of 1200 s in cerium solution. Uniform surface with mud-crack morphology was obtained in the cerium conversion coating. These features were also related to the drying process performed after the samples were withdrawn of the conversion bath. No strict relation was reported with the inter-metallics as they are distributed in the entire surface (Johansen et al., 2012). The EDX analysis of the cerium conversion coating is presented in Figure 1c, and the relevant cerium content was obtained to be 14.1 wt.%.

3.2. Potentiodynamic polarization measurements

The electrochemical properties the cerium oxide coatings at different immersion times were studied using potentiodynamic polarization. The polarization curves of cerium oxide coated AA2024 electrode are shown in Figure 2. Table 1 also shows the corrosion parameters like corrosion potential (E_{corr}). It can be seen that, by applying cerium oxide films, the current density of corrosion decreased, which confirms the inhibiting behavior of the cerium oxide coatings on the AA2024 substrate. It can also be seen that, by an increase in immersion time from 30 to 1800 s, I_{corr} and the corrosion rate of the coated samples decreased. By increasing cerium oxide immersion time up to 1200 s, propagation on surface increased and covered all the surface. By taking out the samples from the solution and performing the drying process at ambient temperature, some cracks progressed on their surface,

thereby leading to a decline in the corrosion resistance of the coatings. The coating upper layer during drying was hardened and water was trapped in inner layer of cerium oxide. Hence, the trapped water cannot be released from the coating because of the existence of the top hard layer, which leads to cracking. Furthermore, after 1200 s immersion time, the current density and rate of corrosion increased, which was attributed to the deep cracks formation because of the high thickness of film, leading to a decrease in its toughness.

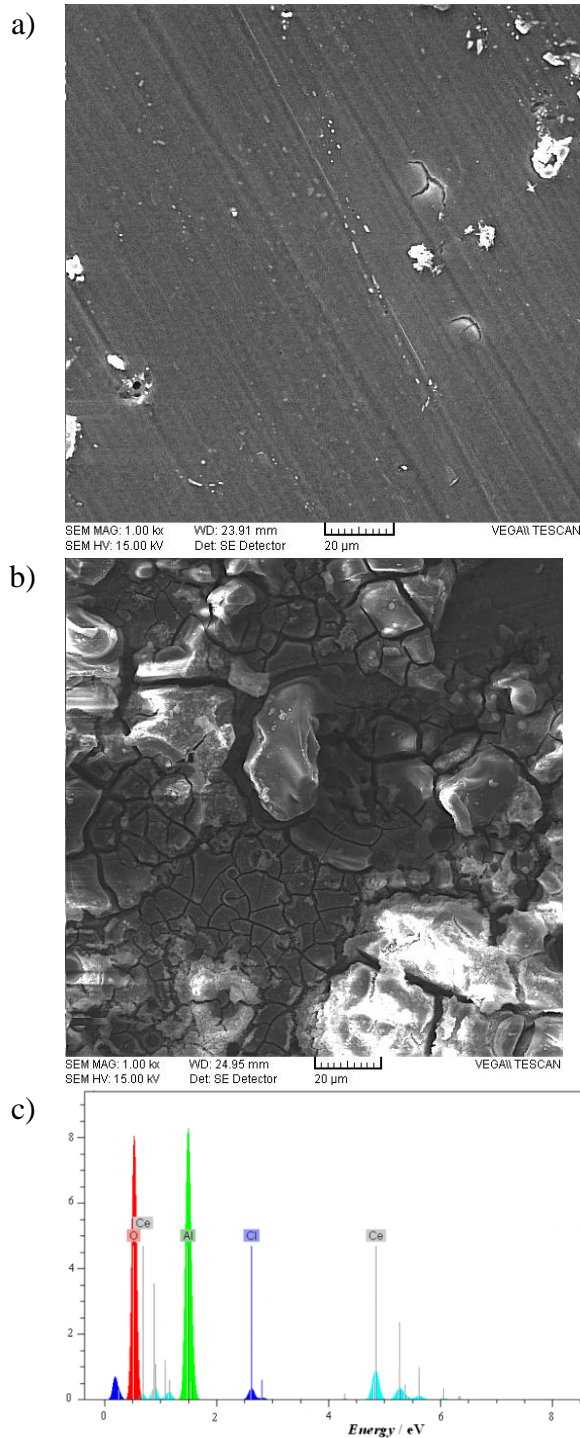


Figure 1
 SEM micrographs of AA2024 samples: a) without and b) with cerium conversion coating obtained after 1200 s immersion; c) EDX analysis of cerium oxide coating.

The results reported in Table 1 show that a more protective layer on aluminum surface is observed when the sample is coated by immersion in cerium for 1200 s. The effect of cerium-based conversion coating on corrosion resistance is more evident in the cathodic polarization plots in comparison with the anodic polarization plots. This is evidence for cerium deposition as an oxide/hydroxide on cathodic places (Hasannejad et al., 2009). By cathodic reactions on the surface of the metal, the anodic reactions are balanced. As also reported in the literature, deposition is due to an increase in local pH made by the cathodic reaction happened by H_2O_2 close to the intermetallic compounds (de Frutos et al., 2008).

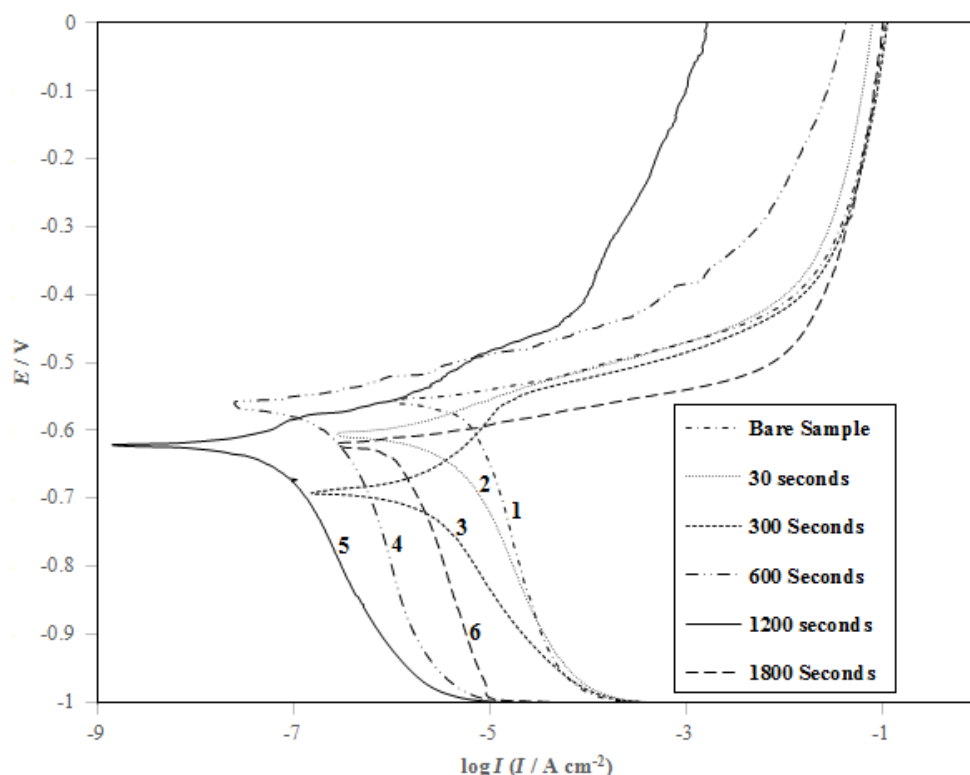


Figure 2

Potentiodynamic polarization curves of cerium-coated AA2024 in a 3.5 wt.% NaCl solution; cerium conversion was obtained at different immersion times: 1) bare, 2) 30 s, 3) 300 s, 4) 600 s, 5) 1200 s, and 6) 1800 s.

3.3. Electrochemical impedance

Electrochemical impedance was employed for the confirmation of the anticorrosion properties of the cerium coating. Figure 3 shows the impedance diagrams of cerium conversion coated AA2024 obtained at different immersion times; at open circuit potential in a 3.5 wt.% NaCl solution, the impedance was measured. The data show that the impedance diagram consists of a depressed capacitive loop because of the double layer capacitance and charge transfer resistance. The equivalent circuit compatible with the Nyquist diagram is depicted in Figure 4. The easiest method needs the theoretical transfer function $Z(\omega)$ to be explained by a resistance parallel combination R_{ct} and a capacitance Q , both in series with another resistance R_s (Jafari et al., 2013):

$$Z(\omega) = R_s + \frac{1}{\frac{1}{R_{ct}} + (i\omega)^n Q} \quad (7)$$

where, ω is the frequency in rad/s and $\omega = 2\pi f$; f is frequency in Hz. R_s , Q_{dl} , and R_{ct} are the solution resistance, a constant phase element relevant to the double layer capacitance, and the charge transfer resistance in this electrical equivalent circuit. In order to obtain a suitable cerium oxide coated aluminum impedance simulation, it is necessary for the capacitor (C) to be replaced with a constant phase element (CPE) Q in the equivalent circuit. Microscopic roughness is an explanation extensively accepted for the existence of depressed semicircles and CPE behavior on solid electrodes, which leads to an inhomogeneous distribution in the solution resistance and in the double-layer capacitance (Gholami et al., 2013). The experimental results were fitted to equivalent circuit, and the circuit elements were obtained to corroborate the equivalent circuit. Table 2 illustrates the equivalent circuit parameters for the impedance spectra of cerium oxide coated aluminum corrosion in NaCl solution. According to Table 2, increasing immersion time raises the charge transfer resistance because of the existence of a more adherent and uniform cerium layer on the AA2024 surface, which will decrease substrate active area. This is continued with a slow decline in impedance at an immersion time of 1800 s because of the larger cracks formation. As the Q_{dl} exponent (n) is a measure of surface heterogeneity, values of n indicate that increasing immersion time results in a more homogenous surface of aluminum due to the corrosion inhibition and uniform coatings.

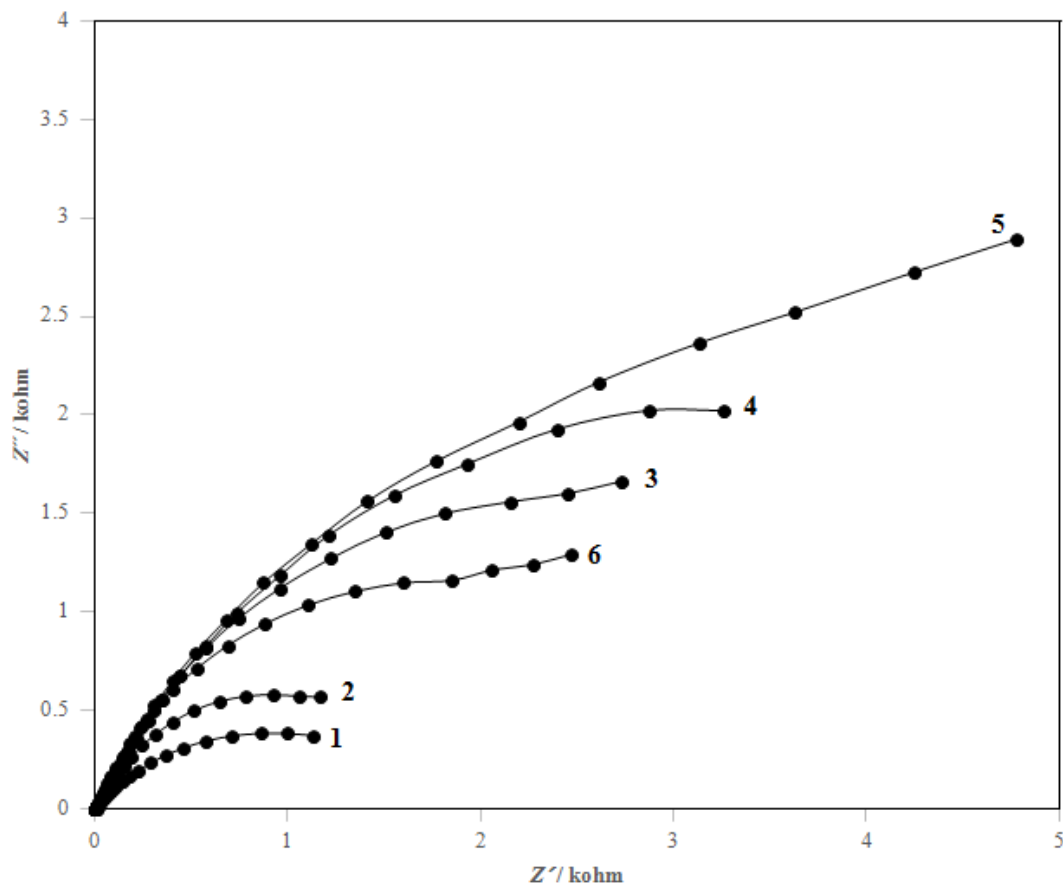


Figure 3

Impedance diagrams of cerium oxide coated aluminum 2024 in a 3.5 wt.% NaCl solution. Cerium coating was obtained at different immersion times in cerium chloride solutions: 1) bare, 2) 30 s, 3) 300 s, 4) 600 s, 5) 1200 s, and 6) 1800 s.

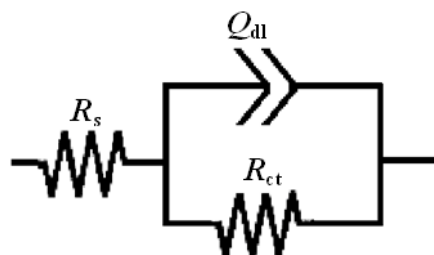


Figure 4

Equivalent circuits compatible with the experimental impedance data in Figure 2.

The time dependency of cerium oxide coated aluminum in NaCl solution is presented in Figure 5. By applying an immersion time of 1200 s cerium conversion coating was obtained. As can be observed, by increasing immersion time up to 24 hrs the charge transfer resistance increases in a corrosive solution. At a higher immersion time, because of the further Cl⁻ penetration to coating layer, and consequently the deterioration of the cerium conversion coatings, the charge transfer resistance declines.

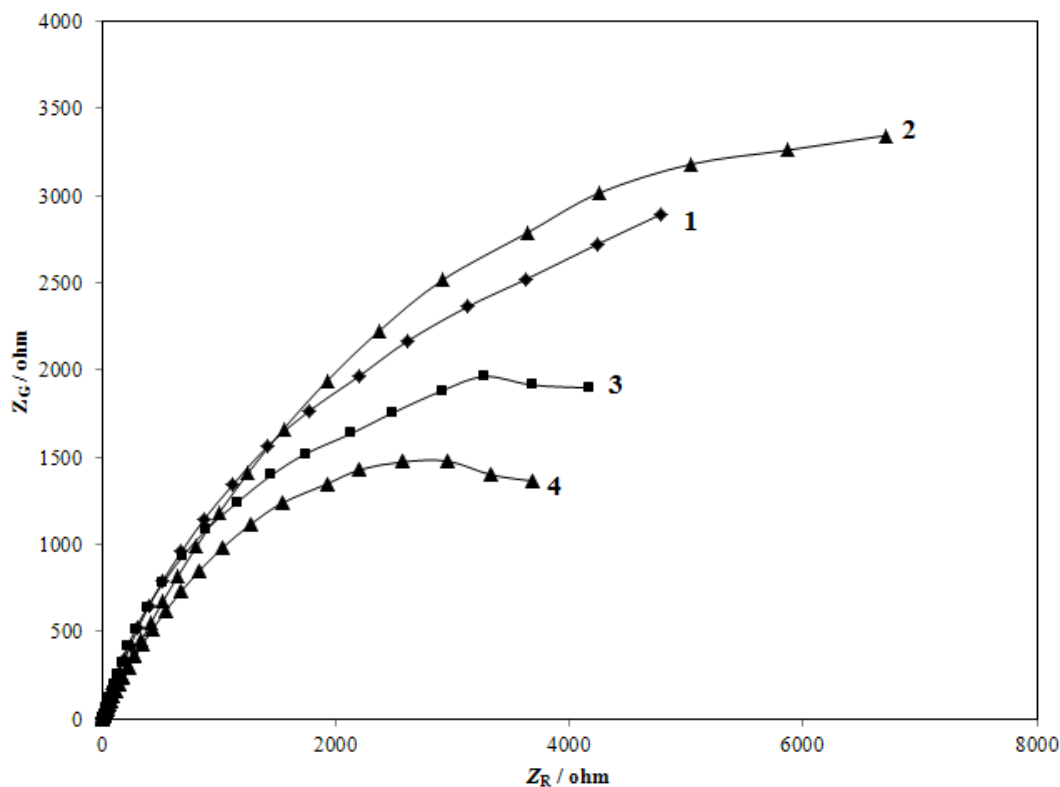


Figure 5

Impedance diagrams of cerium oxide coated aluminum 2024 at different immersion times in a 3.5 wt.% NaCl solution: 1) 30 min, 2) 24 hrs, 3) 48 hrs, and 4) 72 hrs. Cerium coating was obtained at an immersion time of 1200 s.

4. Conclusions

The electrochemical properties of AA2024 aluminum alloy coated with cerium conversion coating were studied in a 3.5 wt.% NaCl solution through electrochemical impedance, potentiodynamic polarization, and SEM-EDS analysis. The cerium-based conversion coating enhanced the alloy

corrosion resistance because it inhibited the cathodic and anodic reactions in a chloride-containing environment. The time of immersion in the cerium solution had an important influence on the corrosion behavior, and the optimum coating behavior was achieved at an immersion time of 1200 s. The coating produced in longer immersion times led to an increase in corrosion rate because of the deep cracks formed in the coating layer.

Nomenclature

I_{corr}	: Corrosion current density
Q_{dl}	: Double layer capacitance
R_{ct}	: Charge transfer resistance
R_p	: Polarization resistance
R_s	: Solution resistance
β_a, β_c	: Tafel slopes

References

- Brunelli, K., Bisaglia, F., Kovac, J., Magrini, M., and Dabalà, M., Effects of Cathodic Electrodeposition Parameters of Cerium Oxide Film on the Corrosion Resistance of the 2024 Al Alloy, *Materials and Corrosion*, Vol. 60, p. 514-520, 2009.
- Campestrini, P., Böhm, S., Schram, T., Terryn, H., and Wit, J. H. W. D., Study of the Formation of Chromate Conversion Coatings on Al Clad 2024 Aluminum Alloy Using Spectroscopic Ellipsometry, *Thin Solid Films*, Vol. 410, p. 76-85, 2002.
- Conde, A., Arenas, M., Frutos, A.D., and Damborenea, J. D., Effective Corrosion Protection of 8090 Alloy by Cerium Conversion Coatings, *Electrochimica Acta*, Vol. 53, p. 7760-7768, 2008.
- De Frutos, A., Arenas, M.A., Liu, Y., Skeldon, P., Thompson, G.E., de Damborenea, J., and Conde, A., Influence of Pre-treatments in Cerium Conversion Treatment of AA2024-T3 and 7075-T6 Alloys, *Surface and Coatings Technology*, Vol. 202, p. 3797-3807, 2008.
- Gholami, M., Danaee, I., Maddahy, M. H., and RashvandAvei, M., Correlated Ab Initio and Electroanalytical Study on Inhibition Behavior of 2-Mercaptobenzothiazole and its Thiole–thione Tautomerism Effect for the Corrosion of Steel (API 5L X52) in Sulfuric Acid Solution, *Industrial and Engineering Chemistry Research*, Vol. 52, p. 14875–14889, 2013.
- Hasannejad, H., Aliofkhazraei, M., Shanaghi, A., Shahrabi, T., and Sabour, A. R., Nanostructural and Electrochemical Characteristics of Cerium Oxide Thin Films Deposited on AA5083-H321 Aluminum Alloy Substrates by Dip Immersion and Sol–gel Methods, *Thin Solid Film*, Vol. 517, p. 4792-4799, 2009.
- Jafari, H., Danaee, I., Eskandari, H., and RashvandAvei, M., Electrochemical and Theoretical Studies of Adsorption and Corrosion Inhibition of N,N-Bis(2-hydroxyethoxyacetophenone)-2,2-dimethyl-1,2-propanediimine on Low Carbon Steel (API 5L Grade B) in Acidic Solution, *Industrial and Engineering Chemistry Research*, Vol. 52, p. 6617-6632, 2013.
- Johansen, H. D., Brett, C. M., and Motheo, A. J., Corrosion Protection of Aluminum Alloy by Cerium Conversion and Conducting Polymer Duplex Coatings, *Corrosion Science* Vol. 63, p. 342-350, 2012.

- Johnson, B., Edington, J., Williams, A., and O'Keefe, M., Microstructural Characteristics of Cerium Oxide Conversion Coatings Obtained by Various Aqueous Deposition Methods, *Materials Characterizations*, Vol. 54, p. 41-48, 2005.
- Macdonald, J. R., Note on the Parameterization of the Constant-phase Admittance Element, *Solid State Ionics*, Vol. 13, p. 147-149, 1984.
- Pinc, W., Yu, P., O'Keefe, M., and Fahrenholtz, W., Effect of Gelatin Additions on the Corrosion Resistance of Cerium Based Conversion Coatings Spray Deposited on Al 2024-T3, *Surface and Coatings Technology*, Vol. 203, p. 3533-3540, 2009.
- Pinc, W., Maddela, S., O'Keefe, M., and Fahrenholtz, W., Formation of Subsurface Crevices in Aluminum Alloy 2024-T3 During Deposition of Cerium-Based Conversion Coatings, *Surface and Coatings Technology*, Vol. 204, p. 4095-4100, 2010.
- Rivera, B. F., Johnson, B. Y., O'Keefe, M. J., and Fahrenholtz, W. G., Deposition and Characterization of Cerium Oxide Conversion Coatings on Aluminum Alloy 7075-T6, *Surface and Coatings Technology*, Vol. 176, p. 349-356, 2004.
- Tang, J., Han, Z., Zuo, Y., and Tang, Y., A Corrosion Resistant Cerium Oxide Based Coating on Aluminum Alloy 2024 Prepared by Brush Plating, *Applied Surface Science*, Vol. 257, p. 2806-2812, 2011.